# White Dwarfs as Dark Matter Detectors

Peter W. Graham,[1] Ryan Janish,[2] Vijay Narayan,[2] Surjeet Rajendran,[2] and Paul Riggins[2]

[1]*Stanford Institute for Theoretical Physics, Department of Physics, Stanford University, Stanford, CA, 94305*
[2]*Berkeley Center for Theoretical Physics, Department of Physics, University of California, Berkeley, CA 94720, USA*

If dark matter (DM) is capable of sufficiently heating a local region in a white dwarf, it will trigger runaway fusion and ignite a type 1a supernova. This was originally proposed in [1] and used to constrain primordial black holes which transit and heat a white dwarf via dynamical friction. In this paper, we extend the analysis of white dwarf DM detection to candidates with non-gravitational interactions that heat through the production of standard model (SM) particles. We analyze the stopping of high-energy SM particles in the WD medium, and find they efficiently thermalize and ignite runaway fusion. We constrain a general class of models in which DM produces SM particles via DM-SM inelastic scatters, DM-DM collisions or DM decays, and consider both DM captured by the star and DM that transits without capture. The constraints are due to the existence of long-lived white dwarfs and the observed supernovae rate. As a concrete example, we rule out supersymmetric Q-ball DM in a large region of parameter space fundamentally inaccessible to terrestrial detection. It is also intriguing that the DM-induced ignition discussed in this work provide an alternative mechanism of triggering supernovae from sub-Chandrasekhar Mass progenitors.

## I. INTRODUCTION

Identifying the nature of dark matter (DM) remains one of the clearest paths beyond the Standard Model (SM) and it is thus fruitful to study the observable signatures of any yet-allowed candidate. Many terrestrial direct detection experiments are designed to search for DM, e.g. [2, 3], yet these lose sensitivity to heavier DM due to its diminished number density. Even for a strongly-interacting candidate, if the DM mass is above $\sim 10^{22}$ GeV a detector of size $\sim (100\text{ m})^2$ will register fewer than one event per year. While these masses are large compared to those of fundamental particles, it is reasonable to suppose that DM may exist as composite states just as the SM produces complex structures with mass much larger than fundamental scales (e.g. you, dear reader). Currently there is a wide range of unexplored parameter space for DM candidates less than $\sim 10^{48}$ GeV, above which the DM will have observable gravitational microlensing effects [4]. For such ultra-heavy DM, indirect signatures in astrophysical systems are a natural way forward. One possibility proposed by [1] is that DM can trigger runaway fusion and ignite type 1a supernovae (SN) in sub-Chandrasekhar white dwarf (WD) stars. This is even more interesting in light of recent observations that an $\mathcal{O}(1)$ fraction of type 1a SN are due to sub-Chandrasekhar progenitors [5, 6]. While astrophysical mechanisms for these events have been proposed [7–9], the situation is yet unclear and it is an exciting possibility that these SN arise from DM interactions.

Runaway thermonuclear fusion requires both a heating event and the lack of significant cooling which might quench the process. The WD medium is particularly suited to this as it is dominated by degeneracy pressure and undergoes minimal thermal expansion, which is the mechanism that regulates fusion in main sequence stars. Thermal diffusion is the primary cooling process in a WD and it can be thwarted by heating a large enough region. The properties of a localized heating necessary to trigger runaway fusion were computed in [10]. Consequently, it was realized [1] that if DM is capable of sufficiently heating a WD in this manner, it will result in a SN with sub-Chandrasekhar mass progenitor. This was used to constrain primordial black holes which transit a WD and cause heating by dynamical friction, although the authors of [1] identify several other heating mechanisms which may be similarly constrained.

In this paper, we examine DM candidates with non-gravitational interactions that cause heating through the production of SM particles. An essential ingredient in this analysis is understanding the length scales over which SM particles deposit energy in a WD medium. We find that most high energy particles thermalize rapidly, over distances shorter than or of order the critical size for fusion. Particle production is thus an effective means of igniting WDs. Constraints on these DM candidates come from either observing specific, long-lived WDs or by comparing the measured rate of type 1a SN with that expected due to DM. It is important to note that these constraints are complementary to direct searches—it is more massive DM that is likely to trigger SN, but also more massive DM that has low terrestrial flux. The WD detector excels in this regime due to its large surface area $\sim (10^4\text{ km})^2$, long lifetime $\sim$ Gyr, and galactic abundance. We demonstrate these constraints for generic classes of DM models that produce SM particles via DM-SM inelastic scattering, DM-DM collisions, or DM decays, and consider the significantly enhanced constraints for DM that is captured in the star. As a concrete example we consider ultra-heavy Q-ball DM as found in supersymmetric extensions of the SM.

The rest of the paper is organized as follows. We begin in Section II by reviewing the mechanism of runaway

fusion in a WD. In Section III we study the heating of a WD due to the production of high-energy SM particles. Detailed calculations of the stopping of such particles are provided in Appendix A. In Section IV we parameterize the explosiveness and event rate for generic classes of DM-WD encounters, and in Section V we derive schematic constraints on such models. The details of DM capture in a WD are reserved for Appendix B. Finally we specialize to the case of Q-balls in Section VI, and conclude in Section VII.

## II. WHITE DWARF RUNAWAY FUSION

We first review the conditions for which a local energy deposition in a WD results in runaway fusion. Any energy deposit will eventually heat ions within some localized region—parameterize this region by its linear size $L_0$, total kinetic energy $\mathcal{E}_0$ and typical temperature $T_0$. These scales evolve in time, but it will be useful to describe a given heating event by their initial values.

The fate of a heated region is either a nonviolent diffusion of the excess energy across the star, or a runaway fusion chain-reaction that destroys the star. The precise outcome depends on $L_0$, $\mathcal{E}_0$ and $T_0$. There is a critical temperature $T_f$, set by the energy required for ions to overcome their mutual Coulomb barrier, above which fusion occurs. For carbon burning, $T_f \sim$ MeV [11]. Any heated region $T_0 > T_f$ will initially support fusion, although this is not sufficient for runaway as cooling processes may rapidly lower the temperature below $T_f$. This cooling will not occur if the corresponding timescale is larger than the timescale at which fusion releases energy. Cooling in a WD is dominated by thermal diffusion, and the diffusion time increases as the size of the heated region. However, the timescale for heating due to fusion is independent of region size. Thus, for a region at temperature $\gtrsim T_f$, there is a critical size above which the heated region does not cool but instead initiates runaway. For a region at the critical fusion temperature $T_f$, we call this critical size the *trigger size* $\lambda_T$. The value of $\lambda_T$ is highly dependent on density, and in a WD is set by the thermal diffusivity of either photons or degenerate electrons. This critical length scale has been computed numerically in [10] for a narrow range of WD densities and analytically scaled for other WD masses in [1]. As in [1], we will restrict our attention to carbon-oxygen WDs in the upper mass range $\sim 0.85 - 1.4\ M_\odot$ (these will yield the most stringent constraints on DM). This corresponds to a central number density of ions $n_{\rm ion} \sim 10^{30} - 10^{32}$ cm$^{-3}$ and a trigger size of $\lambda_T \sim 10^{-3} - 10^{-5}$ cm.

If a heated region is smaller than the trigger size, its thermal evolution is initially dominated by diffusion. However, this will still result in runaway fusion if the temperature is of order $T_f$ by the time the region diffuses out to the trigger size. For our purposes it is more natural to phrase this in terms of the total energy $\mathcal{E}_0$ deposited during a heating event. Of course, the relation between energy $\mathcal{E}_0$ and temperature $T_0$ depends on the rate at which WD constituents—ions, electrons, and photons—thermalize with each other within the region size $L_0$. Given that the different species thermalize rapidly, the excess energy required to raise the temperature to $T_f$ in a volume $V$ is given by a sum of their heat capacities

$$\frac{\mathcal{E}_0}{V} \gtrsim \int_0^{T_f} dT (n_{\rm ion} + n_e^{2/3} T + T^3), \tag{1}$$

where $n_e$ is the number density of electrons. Note that we use the heat capacity of a degenerate gas of electrons, since the Fermi energy $E_F \gtrsim$ MeV for the densities we consider. The minimum energy deposit necessary to trigger runaway fusion is simply

$$\begin{aligned} \mathcal{E}_{\rm boom} &\sim \lambda_T^3 (n_{\rm ion} T_f + n_e^{2/3} T_f^2 + T_f^4) \\ &\approx 10^{15} - 10^{23}\ \text{GeV}. \end{aligned} \tag{2}$$

$\mathcal{E}_{\rm boom}$ varies with $\lambda_T$ over the range of WD densities and is plotted in Figure 1. Thus for a heating event characterized by its $L_0$, $\mathcal{E}_0$, and $T_0 \gtrsim T_f$, there is an *ignition condition*:

$$\mathcal{E}_0 \gtrsim \mathcal{E}_{\rm boom} \cdot \max\left\{1, \frac{L_0}{\lambda_T}\right\}^3. \tag{3}$$

Any $\mathcal{E}_0$ satisfying this condition is minimized for $L_0$ less than the trigger size, where it is also independent of the precise value of $L_0$. For broader deposits, the necessary energy is parametrically larger than $\mathcal{E}_{\rm boom}$ by a volume ratio $(L_0/\lambda_T)^3$. As a result, understanding the $L_0$ for different kinds of heating events in a WD is critical to determining whether or not they are capable of destroying the star.

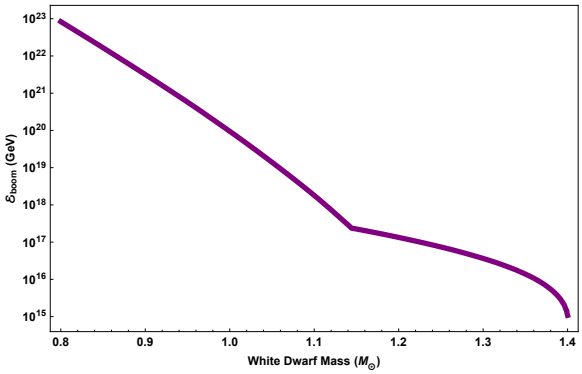


FIG. 1: The minimum energy deposit (2) necessary to trigger runaway fusion, based on numerical results for $\lambda_T$ [10] and the WD mass-density relation [12]

.

## III. PARTICLE HEATING OF WHITE DWARFS

Production of high-energy SM particles in a WD will result in heating of the stellar medium. The critical quantity to understand is the length scale over which such heating occurs—this scale determines the efficiency of the heating event in triggering runaway fusion, as described by condition (3). Note that this is a question of purely SM physics. The unknown physics of DM will serve only to set the initial properties of the SM particles.

We find that SM particles efficiently heat the WD regardless of species or energy (neutrinos are a slight exception)—the heating length is typically less than or of order the trigger size $\lambda_T$. This is accomplished primarily through hadronic showers initiated by collisions with carbon ions. In some cases electromagnetic showers are important, however at high energies these are suppressed by density effects and even photons and electrons are dominated by hadronic interactions. These showers rapidly stop high-energy particles due to their logarithmic nature, transferring the energy into a cloud of low-energy particles which heat the medium through elastic scatters. A schematic for the flow of energy during deposition is given in Figure 2. In this light, the WD operates analogously to a particle detector, including hadronic and electromagnetic "calorimeter" components. Runaway fusion provides the necessary amplification to convert a detected event into an observable signal.

The remainder of this section will discuss the above heating process in more detail. We summarize the dominant source of energy loss and the resulting stopping lengths $\lambda$ for SM particles of incident kinetic energy $\epsilon$, approximated by

$$\lambda \sim \frac{\epsilon}{dE/dx}, \tag{4}$$

where $dE/dx$ is the stopping power in the WD medium. Stopping lengths are plotted in Figures 3 and 4, and a detailed treatment of the stopping powers is given in Appendix A. We will consider incident light hadrons, photons, electrons, and neutrinos—as we are concerned with triggering runaway fusion, we restrict our attention to energies $\epsilon \gg T_f \sim$ MeV.

### A. High-Energy Showers

*a. Hadronic Showers.* Incident hadrons with kinetic energy larger than the nuclear binding scale $\sim 10$ MeV will undergo violent inelastic collisions with carbon ions resulting in an $\mathcal{O}(1)$ number of secondary hadrons. This results in a roughly collinear shower of hadrons of size

$$\begin{aligned} X_{\rm had} &\sim \frac{1}{n_{\rm ion}\sigma_{\rm inel}} \log\left(\frac{\epsilon}{10\ \text{MeV}}\right) \\ &\approx 10^{-6}\ \text{cm} \left(\frac{10^{32}\ \text{cm}^{-3}}{n_{\rm ion}}\right). \end{aligned} \tag{5}$$

where the inelastic nuclear cross section is $\sigma_{\rm inel} \approx 100$ mb and we have taken the logarithm to be $\sim 10$. The shower terminates into pions and nucleons of energy $\sim 10$ MeV, whose cooling is discussed below. Note that neutral pions of

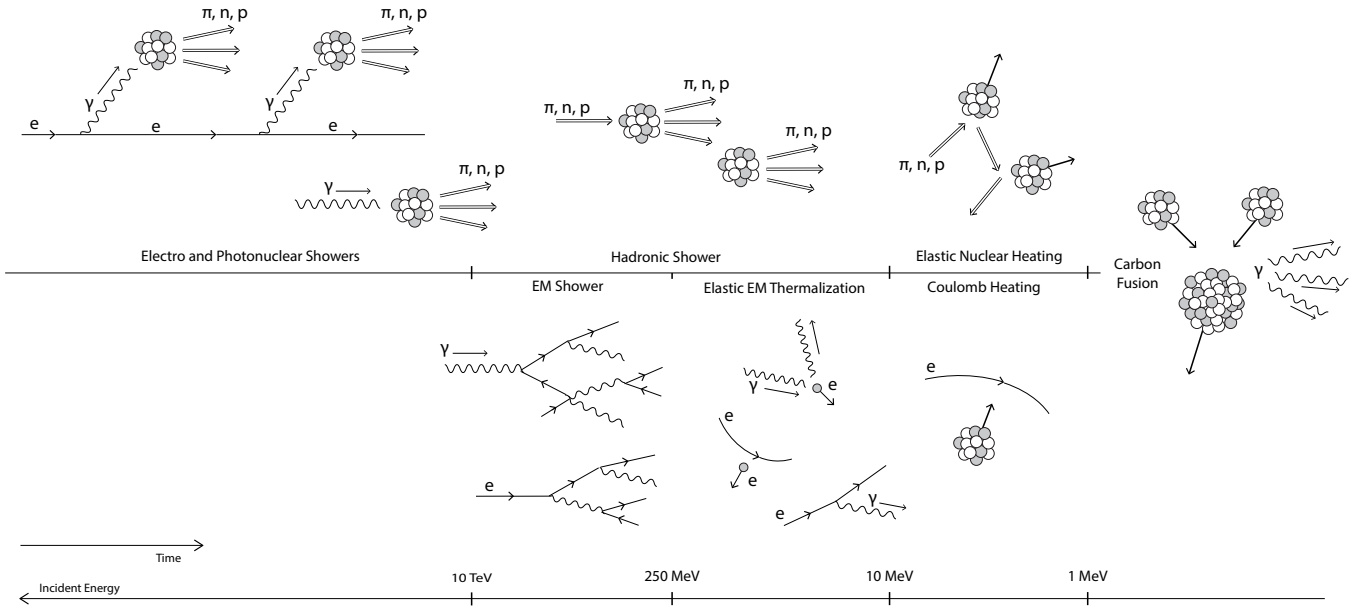


FIG. 2: Dominant energy loss and thermalization processes in the WD as a function of energy, with energy decreasing towards the right. Hadronic processes are shown in the upper panel and EM processes in the lower panel. High energy particles will induce showers that terminate into elastic thermalization of the WD ions, moving from left to right in the diagram. The quoted energies are for a $\sim 1.37\ M_\odot$ WD, although the cartoon is qualitatively the same for all densities.

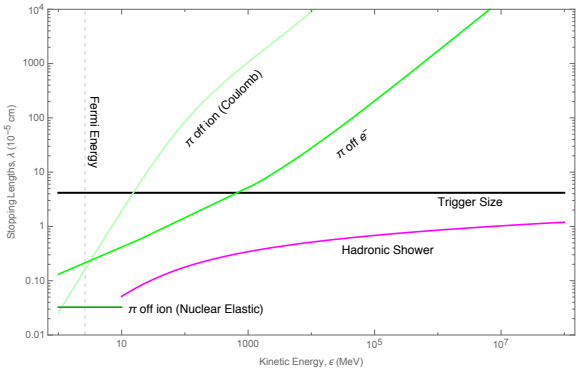


FIG. 3: Stopping lengths for incident hadrons as a function of kinetic energy in a WD of density $n_{\rm ion} \sim 10^{31}\ {\rm cm}^{-3}$ ($\approx 1.25\ M_\odot$), including the hadronic shower length (magenta). Any discontinuities in the stopping lengths are due to approximate analytic results in the different energy regimes. See Appendix A for calculation details.

energy $10 - 100$ MeV have a decay length to photons of $\delta_{\pi^0} \sim 10^{-6}$ cm. Hadronic showers will therefore generate an electromagnetic component carrying an $\mathcal{O}(1)$ fraction of the energy.

*b. Photonuclear and Electronuclear Showers.* A photon or electron can directly induce hadronic showers via production of a quark-antiquark pair, depicted in Figure 5. The LPM effect, discussed below, ensures that these process dominate the stopping of photons and electrons at high energies, $\epsilon \gtrsim 10^4 - 10^6$ GeV.

The only substantial difference between photonuclear showers and purely hadronic ones is that they require a longer distance to initiate. Roughly, the photonuclear cross section is suppressed relative to the hadronic inelastic cross section $\sigma_{\rm inel}$ by a factor of $\alpha$, and so the photon range is

$$\lambda_{\gamma A} \approx 10^{-5}\ {\rm cm} \left( \frac{10^{32}\ {\rm cm}^{-3}}{n_{\rm ion}} \right). \tag{6}$$

Here $\lambda_{\gamma A}$ is the distance to initiate a hadronic shower, whereas the shower itself extends a distance $X_{\rm had}$. Note that $\lambda_{\gamma A}$ is of order the trigger size.

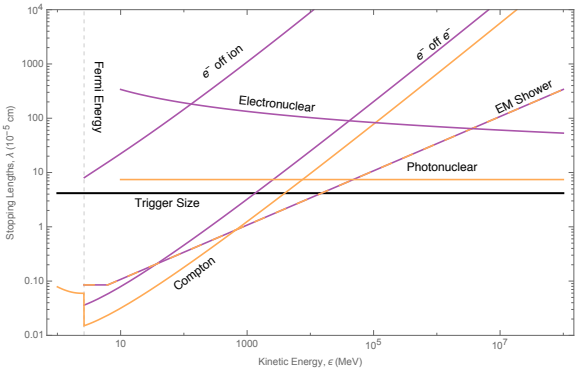


FIG. 4: Stopping lengths of incident photons (orange) and electrons (purple) as a function of kinetic energy in a WD of density $n_{\rm ion} \sim 10^{31}$ cm$^{-3}$ ($\approx 1.25\ M_\odot$), including the EM shower length (dashed). Any discontinuities in the stopping lengths are due to approximate analytic results in the different energy regimes. See text for calculation details.

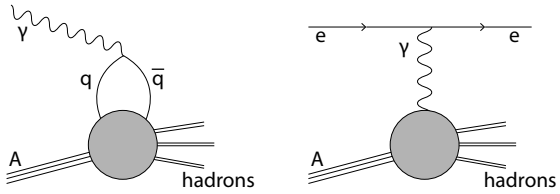


FIG. 5: Photonuclear (left) and Electronuclear (right) interactions. The shaded region contains, at high energies, the familiar point-like processes of deep inelastic scattering and for energies below $\Lambda_{\rm QCD}$ is best described by exchange of virtual mesons.

The electronuclear showers are qualitatively different, as the electron survives the interaction. This process is best described as a continuous energy loss of the electron, due to radiation of virtual photons into hadronic showers. The stopping power is again radiative, which gives the constant stopping length

$$\lambda_{eA} \approx 10^{-4}\ {\rm cm} \left(\frac{10^{32}\ {\rm cm}^{-3}}{n_{\rm ion}}\right). \tag{7}$$

This is suppressed by an additional factor of $\alpha$ relative to the photonuclear interaction, although a full calculation also yields an $\mathcal{O}(10)$ logarithmic enhancement. We see that the electronuclear length scale $\lambda_{eA}$ is at most larger than the trigger size by an order of magnitude.

*c. Electromagnetic Showers.* Of course, electrons and photons can also shower through successive bremsstrahlung and pair-production. An electromagnetic shower proceeds until a critical energy $\sim 100$ MeV, at which point these radiative processes become subdominant to elastic Coulomb and Compton scattering. Below this scale radiation can still be important, though electromagnetic showers do not occur. Note that bremsstrahlung and pair-production are strictly forbidden for incident energies below the Fermi energy $E_F$.

At sufficiently high electron/photon energies and nuclear target densities, electromagnetic showers are elongated due to the "Landau-Pomeranchuk-Migdal" (LPM) effect. High-energy radiative processes necessarily involve small momentum transfers to nuclei. These soft virtual photons cannot be exchanged with only a single ion, but rather interact simultaneously with multiple ions. This generates a decoherence, suppressing bremsstrahlung/pair-production above an energy $E_{\rm LPM}$ which scales inversely with density:

$$E_{\rm LPM} \approx 1\ {\rm MeV} \left(\frac{10^{32}\ {\rm cm}^{-3}}{n_{\rm ion}}\right) \tag{8}$$

The corresponding shower lengths are

$$X_{\rm EM} \approx X_0 \cdot \begin{cases} \left(\frac{\epsilon}{E_{\rm LPM}}\right)^{1/2} & \epsilon > E_{\rm LPM} \\ 1 & \epsilon < E_{\rm LPM} \end{cases} \tag{9}$$

where

$$X_0 \approx 10^{-7}\ \text{cm} \left(\frac{10^{32}\ \text{cm}^{-3}}{n_{\text{ion}}}\right). \tag{10}$$

is the unsuppressed EM shower length. See Appendix A 3 for details. At the highest WD densities radiative processes are always LPM-suppressed, while at lower densities we observe both regimes. We emphasize that for all densities, throughout the energy range where it is relevant, the length of electromagnetic showers is never parametrically larger than the trigger size.

*d. Neutrinos.* Neutrinos scatter off nuclei with a cross section that increases with energy. In these interactions, an $\mathcal{O}(1)$ fraction of the neutrino energy is transferred to the nucleus with the rest going to produced leptons—this is sufficient to start a hadronic shower [13, 14]. At an energy of $\sim 10^{11}$ GeV, [13] calculates the neutrino-nuclear cross section to be $\sim 10^{-32}$ cm$^2$. Conservatively assuming this value for even higher energies, we find a neutrino mean free path in a WD of order $\sim 10$ cm. While this distance is much too large to heat a WD via the release of multiple low-energy neutrinos, for a single neutrino it is simply a displacement after which a compact shower of size $X_{\text{had}}$ occurs. As such, a *single* high-energy neutrino will heat the star just as high-energy hadrons do.

### B. Low-Energy Elastic Heating

The showers of high-energy particles described above terminate in a cloud of low-energy $\epsilon \sim 10$ MeV neutrons, protons, and charged pions, and $\epsilon \sim 10 - 100$ MeV electrons and photons. Of course, particles at these energies may also be directly produced by the DM. At these energies, elastic nuclear, Coulomb, and Compton scatters dominate and eventually lead to the thermalization of ions.

*a. Hadrons.* Neutral hadrons are the simplest species we consider, interacting at low-energies only through elastic nuclear scatters with cross section $\sigma_{\text{el}} \approx$ b. Note that the large ion mass requires $\sim 10 - 100$ scatters to transfer the hadron's energy in the form of a random-walk. This elastic heating range is

$$\lambda_{\text{el}} \approx 10^{-7}\ \text{cm} \left(\frac{10^{32}\ \text{cm}^{-3}}{n_{\text{ion}}}\right), \tag{11}$$

and is always less than the trigger size.

Charged hadrons are also subject to Coulomb interactions, which would provide the dominant stopping in terrestrial detectors. In this case, however, Coulomb scatters off degenerate WD electrons are strongly suppressed and charged hadrons predominantly undergo elastic nuclear scatters like their neutral brethren. This suppression is due to (1) motion of the electrons, which fixes the relative velocity to be $\mathcal{O}(1)$ and removes the enhancement of Coulomb stopping usually seen at low velocity, and (2) Pauli blocking, which forces the incident particle to scatter only electrons near the top of the Fermi sea. For an incident particle with velocity $v_{\text{in}} \ll 1$, the first effect suppresses the stopping power by a factor of $v_{\text{in}}^2$ relative to that off stationary, non-degenerate electrons and the second by an additional factor of $v_{\text{in}}$. Note that there is a small range of energies in which Coulomb scatters off ions dominate the stopping of charged hadrons—either way, both length scales are well below the trigger size.

*b. Electrons and Photons.* For electrons and photons below $\sim 100$ MeV the dominant interactions are Coulomb scatters off WD electrons and Compton scatters, respectively. The length scale of these processes is smaller than any interaction with ions, and so these electrons and photons will thermalize into a compact electromagnetic "gas" with a size set by the radiative length scale $X_{\text{EM}}$. The EM gas will cool and diffuse to larger length scales, eventually allowing thermalization with nuclei via the subdominant Coulomb scatters of electrons off ions. The photons of the EM gas will not undergo photonuclear showers here, as the gas will cool below $\sim 10$ MeV by the time it diffuses out to a size $\lambda_{\gamma A}$. This gas temperature is initially at most $\sim 100$ MeV. At these temperatures the heat capacity is dominated by photons, so as the gas diffuses to a size $\lambda_{\gamma A}$ it cools by a factor $(X_{\text{EM}}/\lambda_{\gamma A})^{3/4} \sim 10^{-2} - 10^{-1}$. Note that for temperatures $T$ less than $E_F$, the electrons are partially degenerate and heating proceeds via the thermal tail with kinetic energies $\epsilon \sim E_F + T$. Therefore, the relevant thermalization process is Coulomb scattering of electrons off ions. This has a stopping length

$$\lambda_{\text{coul}} \approx 10^{-5}\ \text{cm} \left(\frac{\epsilon}{10\ \text{MeV}}\right) \left(\frac{10^{32}\ \text{cm}^{-3}}{n_{\text{ion}}}\right) \tag{12}$$

which is of order the trigger size.

## IV. DARK MATTER-INDUCED IGNITION

Any DM interaction that produces SM particles in a WD has the potential to ignite the star, provided that sufficient SM energy is produced. The distribution in space, momentum, and species of these SM products is dependent on unknown DM physics and is needed to determine the rate of DM-induced ignition. This can be done precisely for a specific DM model, as we do for Q-balls in Section VI. In this Section, however, we study some general features of DM-WD encounters involving DM that possesses interactions with itself and the SM. We collect below the basic formulas relating DM model parameters to ignition criteria, SN rate, etc.

DM can generically produce SM particles in the WD through three basic processes: DM-SM inelastic scattering, DM-DM collisions, and DM decays. For ultra-heavy DM, these processes can be complicated events involving many (possibly dark) final states, analogous to the interactions of heavy nuclei. We classify DM candidates into three types according to the interaction that provides the dominant source of heating, and refer to these as inelastic scattering, collision, and decay candidates. We also make the simplifying assumption that the above events are "point-like", producing SM products in a localized region (smaller than the heating length) near the interaction vertex. If this is not the case (as with some large Q-balls, see Section VI), then the same formalism applies but with the event size added to the stopping length.

The SN rate may be greatly enhanced if DM is captured in the star, so we also consider separately "transiting DM" and "captured DM". In general, there is some loss of DM kinetic energy in the WD. In the transit scenario, this energy loss is negligible and the DM simply passes through the star. In the capture scenario, the energy loss is not directly capable of ignition but is sufficient to stop the DM and cause it to accumulate in the star. Energy loss may be due to a variety of processes, but for simplicity we will focus on an elastic scattering of DM off carbon ions. Of course, due to the velocity spread of DM in the rest frame of a WD, there will necessarily be both transiting and captured DM populations in the star.

### A. DM Transit

*a. DM-SM Inelastic Scattering.* Runaway fusion only occurs in the degenerate WD interior where thermal expansion is suppressed as a cooling mechanism. The outer layers of the WD, however, are composed of a non-degenerate gas and it is therefore essential that a DM candidate penetrate this layer in order to ignite a SN. We parameterize this by a DM stopping power $(dE/dx)_{\rm SP}$, the kinetic energy lost by the DM per distance traveled in the non-degenerate layer, and demand that

$$\left(\frac{dE}{dx}\right)_{\rm SP} \ll \frac{m_\chi v_{\rm esc}^2}{R_{\rm env}}. \tag{13}$$

Here $R_{\rm env} \sim 50$ km is the width of a non-degenerate WD envelope—the density in this region is typically a small fraction $\sim 10^{-3}$ of the central density [15].

DM-SM scattering will result in a continuous energy deposit along the DM trajectory (if the interaction is rare enough for this not to be true, then the encounter is analogous to the case of DM decay). This is best described by a linear energy transfer $(dE/dx)_{\rm LET}$, the kinetic energy of SM particles produced per distance traveled by the DM. If these products have a heating length $L_0$ then the energy deposit must at minimum be taken as the energy transferred along a distance $L_0$ of the DM trajectory. Importantly, as per the ignition condition (3), such a deposition is *less* explosive unless $L_0$ is smaller than the trigger size $\lambda_T$. We thus consider the energy deposited over the larger of these two length scales. Assuming the energy of the DM is roughly constant during this heating event, the ignition condition is:

$$\left(\frac{dE}{dx}\right)_{\rm LET} \gtrsim \frac{\mathcal{E}_{\rm boom}}{\lambda_T} \cdot \max\left\{\frac{L_0}{\lambda_T}, 1\right\}^2. \tag{14}$$

Note that the DM stopping power $(dE/dx)_{\rm SP}$ and the linear energy transfer $(dE/dx)_{\rm LET}$ are possibly controlled by different physics and may have very different numerical values. In addition, a transit event satisfying condition (13) will have negligible energy loss over the parametrically smaller distances $\lambda_T$ or $L_0$, validating (14).

The above condition sums the individual energy deposits along the DM trajectory as though they are all deposited simultaneously. This is valid if the DM moves sufficiently quickly so that this energy does not diffuse out of the region of interest before the DM has traversed the region. We therefore require that the diffusion time $\tau_{\rm diff} \sim 10^{-12}$ s across a heated region of size $L$ at temperature $T_f$ be larger than the DM crossing-time:

$$\tau_{\rm diff} \sim \frac{L^2}{\alpha(T_f)} \gg \frac{L}{v_{\rm esc}}, \tag{15}$$

where $\alpha(T)$ is the temperature-dependent diffusivity, and the DM transits at the stellar escape velocity $v_{\rm esc} \sim 10^{-2}$. This condition is more stringent for smaller regions, so we focus on the smallest region of interest, $L = \lambda_T$. Then (15) is equivalent to demanding that the escape speed is greater than the conductive speed of the fusion wave front, $v_{\rm cond} \sim \alpha(T_f)/\lambda_T$. Numerical calculations of $v_{\rm cond}$ are tabulated in [10], and indeed condition (15) is satisfied for all WD densities.

The rate of transit events is directly given by the flux of DM through a WD

$$\Gamma_{\rm trans} \sim \frac{\rho_\chi}{m_\chi} R_{\rm WD}^2 \left(\frac{v_{\rm esc}}{v_{\rm halo}}\right)^2 v_{\rm halo}, \tag{16}$$

where $\rho_\chi$ is the DM density in the region of the WD, and $R_{\rm WD}$ is the WD radius. Here $v_{\rm halo} \sim 10^{-3}$ is the virial velocity of our galactic halo. Note the $(v_{\rm esc}/v_{\rm halo})^2 \sim 100$ enhancement due to gravitational focusing.

We will not consider here captured DM that heats the star via scattering events, as such heating will typically cause ignition before capture occurs. However, it is possible to cause ignition after capture if the collection of DM leads to an enhanced scattering process.

*b. DM-DM Collisions and DM Decays.* For a point-like DM-DM collision or DM decay event releasing particles of heating length $L_0$, ignition will occur if the total energy in SM products satisfies condition (3). Such an event will likely result in both SM and dark sector products, so we parameterize the resulting energy in SM particles as a fraction $f_{\rm SM}$ of the DM mass. For non-relativistic DM, the DM mass is the dominant source of energy and therefore $f_{\rm SM} \lesssim 1$ regardless of the interaction details. A single DM-DM collision or DM decay has an ignition condition:

$$m_\chi f_{\rm SM} \gtrsim \mathcal{E}_{\rm boom} \cdot \max\left\{\frac{L_0}{\lambda_T}, 1\right\}^3. \tag{17}$$

Thus the WD is sensitive to annihilations/decays of DM masses $m_\chi > 10^{15}$ GeV.

DM that is not captured traverses the WD in a time $t_{\rm ff} \sim R_{\rm WD}/v_{\rm esc}$, and the rate of DM-DM collisions within the WD parameterized by cross-section $\sigma_{\chi\chi}$ is:

$$\Gamma_{\rm ann} \sim \left(\frac{\rho_\chi}{m_\chi}\right)^2 \sigma_{\chi\chi} \left(\frac{v_{\rm esc}}{v_{\rm halo}}\right)^3 v_{\rm halo} R_{\rm WD}^3. \tag{18}$$

Similarly the net DM decay rate inside the WD parameterized by a lifetime $\tau_\chi$ is:

$$\Gamma_{\rm decay} \sim \frac{1}{\tau_\chi}\frac{\rho_\chi}{m_\chi}\left(\frac{v_{\rm esc}}{v_{\rm halo}}\right) R_{\rm WD}^3. \tag{19}$$

### B. DM Capture

*a. Review of DM Capture.* We first summarize the capture and subsequent evolution of DM in the WD, ignoring annihilations or decays—see Appendix B for details. Consider a spin-independent, elastic scattering off ions with cross section $\sigma_{\chi A}$. The rate of DM capture in gravitating bodies is of course very well-studied [18, 19]. However, this rate must be modified when the DM requires multiple scatters to lose the necessary energy for capture. Ultimately, for DM massive enough to ignite and not ruled out by direct detection experiments,the capture rate is of the form

$$\Gamma_{\rm cap} \sim \Gamma_{\rm trans} \cdot \left(n_{\rm ion}\sigma_{\chi A} R_{\rm WD} \frac{m_{\rm ion} v_{\rm esc}^2}{m_\chi v_{\rm halo}^2}\right). \tag{20}$$

Once DM is captured, it eventually thermalizes with the stellar medium to a velocity

$$v_{\rm th} \approx 10^{-12}\left(\frac{m_\chi}{10^{16}\ {\rm GeV}}\right)^{-1/2}, \tag{21}$$

and settles at the thermal radius

$$R_{\rm th} \approx 0.1\ {\rm cm}\left(\frac{m_\chi}{10^{16}\ {\rm GeV}}\right)^{-1/2}. \tag{22}$$

This proceeds in two stages. Captured DM will initially be found on a large, bound orbit that decays after many transits of the WD until the orbital size is fully contained within the star. The DM then completes many orbits within

the star until its orbital size decays to the thermal radius. Subsequently the DM will begin steadily accumulating at $R_{\rm th}$, with the possibility of self-gravitational collapse if the collected mass of DM exceeds the WD mass within this volume. Of course, not all of these stages may be reached within the age of the WD $\tau_{\rm WD} \sim 5$ Gyr. The timescales of the two thermalization stages are

$$t_1 \sim 10^{15}\ {\rm s} \left(\frac{m_\chi}{10^{16}\ {\rm GeV}}\right)^{3/2} \left(\frac{\sigma_{\chi A}}{10^{-35}\ {\rm cm}^2}\right)^{-3/2}, \tag{23}$$

$$t_2 \sim 10^{13}\ {\rm s} \left(\frac{m_\chi}{10^{16}\ {\rm GeV}}\right) \left(\frac{\sigma_{\chi A}}{10^{-35}\ {\rm cm}^2}\right)^{-1}, \tag{24}$$

while the timescale for the onset of self-gravitation (once DM has sunk to $R_{\rm th}$) is

$$t_{\rm sg} \sim 10^{9}\ {\rm s} \left(\frac{m_\chi}{10^{16}\ {\rm GeV}}\right)^{-1/2} \left(\frac{\sigma_{\chi A}}{10^{35}\ {\rm cm}^2}\right)^{-1}. \tag{25}$$

The full time to collect and begin self-gravitating is $t_1 + t_2 + t_{\rm sg}$. This is less than the age of WD if

$$\sigma_{\chi A} \gtrsim 10^{-35}\ {\rm cm}^2 \left(\frac{m_\chi}{10^{16}\ {\rm GeV}}\right). \tag{26}$$

Importantly, for DM masses $m_\chi > 10^{15}$ GeV self-gravitation sets in instantly relative to thermalization. Note that constraints from direct detection [17] demand that the DM-nuclei scattering cross section be sufficiently small

$$\sigma_{\chi A} \lesssim 10^{-29}\ {\rm cm}^2 \left(\frac{m_\chi}{10^{16}\ {\rm GeV}}\right). \tag{27}$$

At any point during the above evolution, captured DM has the potential to trigger a SN. Of particular interest is the ability of DM to ignite a WD during self-gravitational collapse, either via annihilations or the formation of a black hole. A collapse can release sufficient energy to trigger SN even with DM masses less than $10^{15}$ GeV. However, such a process involves additional subtleties beyond the scope of this paper and is the focus of forthcoming work [21]. In the following, we require that a single collision or decay is sufficient to ignite the star, and give only a quick assessment of collapse.

*b. Captured DM-DM Collisions.* We now turn to the rate of DM-DM collisions for captured DM. Of course, the thermalizing DM constitutes a number density of DM throughout the WD volume. Assuming the scattering cross section satisfies (26) and (27), the total rate of annihilations for this "in-falling" DM is peaked near the thermal radius and is of order:

$$\Gamma_{\rm infall} \sim \frac{(\Gamma_{\rm cap} t_2)^2}{R_{\rm th}^3} \sigma_{\chi\chi} v_{\rm th}. \tag{28}$$

If $\Gamma_{\rm infall} t_2 > 1$, then a SN will be triggered by the in-falling DM population—otherwise, a collapse will proceed. As we will see, ignition of a WD during collapse is almost guaranteed unless $\sigma_{\chi\chi}$ is sufficiently small. When the DM sphere is at a radius $r$, the rate of annihilations is

$$\Gamma_{\rm collapse} \sim \frac{(\rho_{\rm WD} R_{\rm th}^3/m_\chi)^2}{r^3} \sigma_{\chi\chi} v_\chi, \tag{29}$$

$$v_\chi \sim \sqrt{\frac{G\rho_{\rm WD} R_{\rm th}^3}{r}}. \tag{30}$$

Here we have conservatively taken the number of collapsing particles to be the self-gravitational threshold—as mentioned in Appendix B, this is an underestimate for such ultra-heavy DM. We also assume the timescale for collapse is set by the DM cooling rate and is thus related to $t_2$—see Appendix B for details. Of course, there may be some stabilizing physics which prevents the DM from collapsing and annihilating below a certain radius, such as formation of a black hole or bound states. To illustrate the stringent nature of the collapse constraint we will simply assume some benchmark stable radius, as in Figure 9. Note that if a single collision has not occurred during collapse, one may additionally examine annihilations of the subsequent in-falling DM down to the stable radius—for simplicity, we do not consider this scenario.

*c. Captured DM Decays.* Lastly, we compute the rate of decays for captured DM, which is simply proportional to the number of DM particles in the WD available for decay at any given instance. In the transit scenario (19), this number is $\sim \Gamma_{\rm trans} t_{\rm ff}$. In the capture scenario, this number is instead determined by the thermalization time within the WD:

$$\Gamma_{\rm decay} \sim \frac{1}{\tau_\chi} \Gamma_{\rm cap} t_2, \tag{31}$$

conservatively assuming that after a thermalization time, the DM quickly collapses and stabilizes to an "inert" core incapable of further decay. If this is not the case, then the captured DM decay rate is given by replacing $t_2 \to \tau_{\rm WD}$ in (31).

## V. DARK MATTER CONSTRAINTS

We now constrain some simplified models of DM which will ignite a WD via one of the processes parameterized in Section IV. These release SM particles that deposit their energy and thermalize ions within a distance described in Section III. First, however, we review how WD observables constrain DM candidates capable of triggering SN.

### A. Review of WD Observables

Following the discussion of [1], our constraints come from (1) the existence of heavy, long-lived white dwarfs, or (2) the measured type 1a SN rate. The typical age of a WD is of order the age of the universe $\sim$ Gyr. RX J0648.04418 is a nearby star and one of the heavier known WDs, with a mass $\sim 1.25\ M_\odot$ [22] and local dark matter density which we take to be $\rho_\chi \sim 0.4$ GeV/cm$^3$. Of course, this is not the only known heavy WD—the Sloan Digital Sky Survey [23] has found 20+ others. The NuStar collaboration has also recently uncovered evidence for the likely existence of heavy WDs near the galactic center [24], where the DM density is assumed to be much greater $\rho_\chi \gtrsim 10^3$ GeV/cm$^3$ [25]. Such heavy candidates are particularly suited for our constraints as the energy deposit necessary to trigger SN (3) is a decreasing function of WD mass. However, less dense white dwarfs are significantly more abundant in the galaxy. Thus, even if a sufficiently massive DM is unable to trigger a violent heating event within the lifetime of a WD, it could still ignite enough lighter WDs to affect the measured SN rate of $\sim 0.3$ per century. The DM-induced SN rate is estimated using the expected number of white dwarfs per galaxy $\sim 10^{10}$ and their mass distribution [23]. Simulations indicate that only WD masses heavier than $\sim 0.85\ M_\odot$ will result in optically visible SN [1]. Therefore, most of the stars exploded in this manner will be in the mass range $\sim 0.85 - 1\ M_\odot$, resulting in weaker SN than expected of typical Chandrasekhar mass WDs.

To summarize, a bound on DM parameters can be placed if either a single explosive event occurs during the lifetime of an observed star such as RX J0648.04418, or the SN rate due to such DM events throughout the galaxy exceeds the measured value. Note that for low-mass WDs dominated by photon diffusion, $\mathcal{E}_{\rm boom}$ is a strong function of WD density. The average density for WDs is typically a factor $\sim 10^{-2} - 10^{-1}$ less than the central density, although it is found that the WD density only changes by an $\mathcal{O}(1)$ fraction from the central value up to a distance $\sim R_{\rm WD}/2$ [26]. Therefore the central density is a valid approximation as long as we consider heating events within this "modified" WD volume. For simplicity, we employ this approach.

### B. Inelastic Scattering Constraints

In order to constrain a DM model with an inelastic scattering interaction, we require that it satisfy the ignition condition (14). This is given in terms of an LET, which parameterizes the ability for DM to release sufficient energy to the star in the form of SM particles. $(dE/dx)_{\rm LET}$ for any realistic DM model would necessarily involve a sum over stellar targets along with species that could be produced, as well as an integral over the produced particle spectrum. However, we will consider a highly simplified interaction in which $\sigma_{Ni\epsilon}$ denotes the cross-section for DM to undergo a "point-like" scatter off a stellar constituent (e.g. ions), producing $N$ particles of SM species $i$ and individual energy $\epsilon$. The LET for this simple interaction is

$$\left(\frac{dE}{dx}\right)_{\rm LET} = n_{\rm ion}\sigma_{Ni\epsilon}N\epsilon. \tag{32}$$

Note that the assumption of a "point-like" interaction requires that the physical size of the DM is much smaller than $\lambda_T$—this is sensible up to masses of order $\sim 10^{47}$ GeV, at which point the gravitational radius of the DM exceeds $\lambda_T$.

Additionally, one may consider the case that the LET $(dE/dx)_{\rm LET}$ and DM stopping power $(dE/dx)_{\rm SP}$ are equal—that is, the DM loses kinetic energy at the same rate as energy is deposited to the WD. While such a statement is certainly not true for all DM models (such as the Q-ball, which liberates binding energy rather than transferring kinetic energy), it provides a useful benchmark to express the envelope-penetration condition (13).

With the above schematic for DM-SM scattering, we constrain the inelastic scattering cross section $\sigma_{Ni\epsilon}$ as a function of DM mass $m_\chi$. This is done in Figure 6 using the different classes of observables described above and for

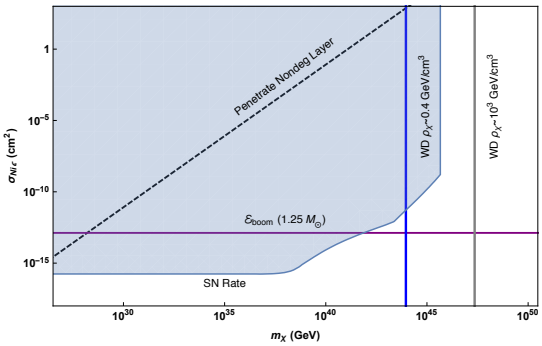


FIG. 6: Constraints on DM-nuclei inelastic scattering cross-section to produce a single SM product (e.g. photon) of energy $\epsilon =$ TeV. Bounds come from demanding that the DM transit triggers runaway fusion (14) (purple), occurs at a rate (16) large enough to either ignite a single observed 1.25 $M_\odot$ WD in its lifetime or exceed the measured SN rate in our galaxy (blue shaded). The dashed line is an example of the envelope-penetration constraint, assuming the energy deposit comes entirely from the DM's kinetic energy.

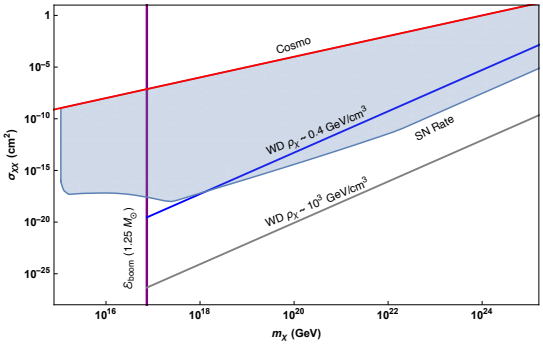


FIG. 7: Constraints on DM-DM collision cross-section to SM products of energy $\epsilon \gg$ MeV. Bounds come from demanding that the DM transit interaction triggers runaway fusion (17) (purple) and occurs at a rate (18) large enough to either ignite a single observed 1.25 $M_\odot$ WD in its lifetime or exceed the measured SN rate in our galaxy (blue shaded). Also shown is the cosmological bound on DM self-interaction (red).

representative choices of $N, \epsilon$. As shown in Section III, the constraint has minimal dependence on the SM species $i$—in the case of neutrinos, we may simply demand that $\epsilon$ is sufficiently large that a single neutrino can ignite the star. Note that the cross sections constrained here are very large—however, these constraints reach to very large masses and are therefore much stronger than existing bounds, e.g. colliding galaxy clusters [29].

### C. Collision and Decay Constraints

In order to constrain a DM model through its annihilations or decays within a WD, we require that it satisfy the ignition condition (17). Consider a simplified interaction wherein a single annihilation or decay releases $N$ particles of SM species $i$ and energy $\epsilon$. Assuming a fractional parameter $f_{\rm SM} = 1$, this corresponds to SM products with individual energy $\epsilon \sim m_\chi/N$. Again, as long as $\epsilon \gg$ MeV there is minimal dependence of the constraints on number of particles $N$ or species $i$ (with the exception of neutrinos).

With this schematic for the DM interaction, we can constrain the cross section for collision $\sigma_{\chi\chi}$ and lifetime $\tau_\chi$. This is done in Figures 7 and 8 in the case of transiting DM using the different classes of observables for DM-DM collisions and DM decays, respectively. In the case of captured DM, we also specify a benchmark value for the elastic scattering cross section $\sigma_{\chi A}$ and, with regards to DM-DM collisions, a stabilizing radius for the collapsing DM sphere. This is done in Figures 9 and 10—for simplicity, here we only show the constraints from the existence of nearby, heavy WDs.

Of course, there are additional limits on DM interactions of this kind complementary to the limits placed from WDs. For one, demanding that the galactic halo has not substantially depleted during its lifetime yields a cosmological bound on DM self-interactions $\frac{\sigma_{\chi\chi}}{m_\chi} < \frac{\rm b}{\rm GeV}$. This is similar in magnitude to the Bullet cluster bounds [29]. There is also a

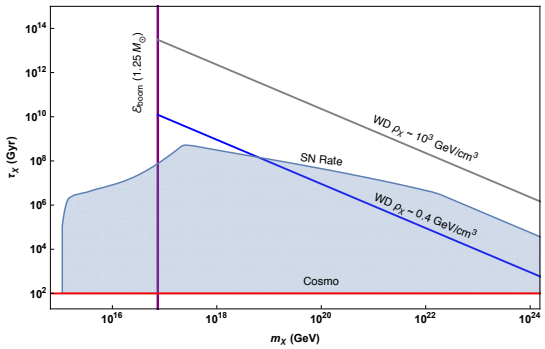


FIG. 8: Constraints on DM decay to SM products of energy $\epsilon \gg$ MeV. Bounds come from demanding that the DM transit interaction triggers runaway fusion (17) (purple) and occurs at a rate (19) large enough to either ignite a single observed 1.25 $M_\odot$ WD in its lifetime or exceed the measured SN rate in our galaxy (blue shaded). Also shown is the cosmological bound on DM lifetime (red).

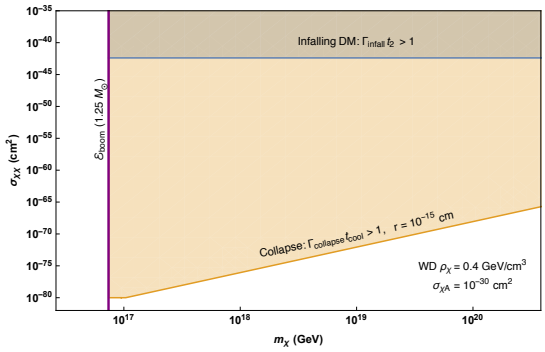


FIG. 9: Constraints on DM-DM collision cross-section to SM products of energy $\epsilon \gg$ MeV, assuming DM is captured with an elastic scattering $\sigma_{\chi A} = 10^{-30}$ cm$^2$. Bounds come from the observation of a single 1.25 $M_\odot$ WD in local DM density. We consider the annihilation rate during the in-falling thermalization stage (28) (blue shaded) and during self-gravitational collapse (29) to a stable radius $r = 10^{-15}$ cm (orange shaded). See text for details.

cosmological bound on DM lifetime $\tau_\chi > 100$ Gyr, independent of the nature of the decay products [30]. In addition, DM annihilations/decays in the galactic halo would contribute to the cosmic ray (CR) flux seen in terrestrial detectors. As CRs of energy greater than $10^{12}$ GeV have not yet been observed [27, 28], this places a bound on DM interaction parameters $\sigma_{\chi\chi}$ and $\tau_\chi$ which involve the release of such ultra-high energy particles. The CR constraint on DM can be estimated by requiring that the expected time for an event to strike earth is less than the typical lifetime of a terrestrial detector $\sim 10$ yr. For a detector of area $\sim (50\ \text{km})^2$ [27], we find that the CR bounds are generally weaker than but within a few orders of magnitude of the WD bounds in the transit scenario. This is actually due to a coincidence in the effective "space-time volumes" of the two systems. A CR detector sees events within a space-time volume ($R_{\rm det}^2 R_{\rm halo} \times 10$ yr) which is comparable to the WD space-time volume ($R_{\rm WD}^3 \times 10^9$ yr), including the additional gravitational enhancement factors. Note that a constraint can also be placed on lower-energy SM products from DM annihilations or decays which would provide an additional source for the measured CR flux, although such an analysis is beyond the scope of this work.

## VI. Q-BALLS

Having derived constraints on generic models of ultra-heavy DM, we turn towards a concrete example. In various supersymmetric extensions of the SM, non-topological solitons called Q-balls can be produced in the early universe [31, 32]. If these Q-balls were stable, they would comprise a component of the DM today. For gauge-mediated models with flat scalar potentials, the Q-ball mass and radius are given by

$$M_Q \sim m_S Q^{3/4}, \quad R_Q \sim m_S^{-1} Q^{1/4}, \tag{33}$$

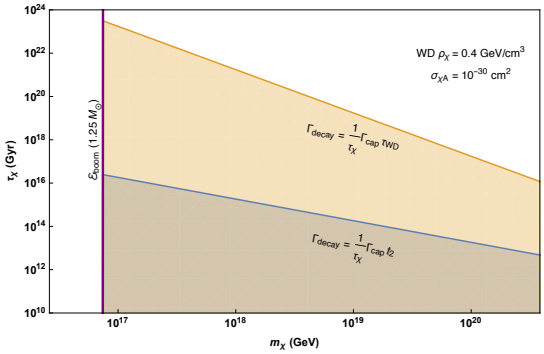


FIG. 10: Constraints on DM decay to SM products of energy $\epsilon \gg$ MeV, assuming DM is captured with an elastic scattering $\sigma_{\chi A} = 10^{-30}$ cm$^2$. Bounds come from the observation of a single 1.25 $M_\odot$ WD in local DM density. We consider the decay rate during the in-falling thermalization stage (31) for gravitational collapse to a non-decaying DM core (blue shaded) or decaying DM core (orange shaded). See text for details.

where $m_S$ is related to the scale of supersymmetry breaking, and $Q$ is the global charge of the Q-ball—in our case, baryon number. The condition $M_Q/Q < m_p$ ensures that the Q-ball is stable against decay to nucleons. When a baryonic Q-ball interacts with a nucleon, it induces the dissociation of the nucleon and absorbs its baryonic charge. During this proton decay-like process, excess energy of order $\Lambda_{\rm QCD}$ is released via the emission of 2–3 pions [33]. We assume that for each Q-ball collision, there is equal probability to produce $\pi^0$ and $\pi^\pm$ under the constraint of charge conservation. The cross section for this interaction is approximately geometric

$$\sigma_Q \sim \pi R_Q^2, \tag{34}$$

and thus grows with increasing $Q$. Note that a sufficiently massive Q-ball will become a black hole if $R_Q \lesssim G M_Q$. In the model described above, this translates into a condition $(M_{\rm pl}/m_S)^4 \lesssim Q$.

We now determine the explosiveness of a Q-ball transit. As in Section V, this process is described by

$$\left(\frac{dE}{dx}\right)_{\rm LET} \sim n_{\rm ion}\sigma_Q N \epsilon, \tag{35}$$

where the nuclear interaction results in $N \sim 30$ pions released, each with kinetic energy $\epsilon \sim 500$ MeV. These pions induce hadronic showers which terminate in low-energy hadrons that rapidly transfer their energy to ions via elastic scatters, as discussed in Section III. The pions have a heating length $X_{\rm had} \lesssim \lambda_T$; however, we will see the Q-ball has a finite size $R_Q \gtrsim X_{\rm had}$ in the region we are able to constrain. So, as mentioned in Section IV, we take the heating length to be $L_0 \sim R_Q + X_{\rm had} \sim R_Q$. The ignition condition is then given by equations (14) and (35):

$$R_Q^2 \gtrsim \frac{1}{n_{\rm ion}} \frac{\mathcal{E}_{\rm boom}}{\lambda_T} \max\left\{\frac{R_Q}{\lambda_T}, 1\right\}^2 \left(\frac{1}{10\ \text{GeV}}\right). \tag{36}$$

This implies $\sigma_Q \gtrsim 10^{-12}$ cm$^2$ is sufficient to ignite a 1.25 $M_\odot$ WD, which corresponds to a charge $Q \gtrsim 10^{42}\ (m_S/\text{TeV})^4$. Note that for sufficiently large $Q$, the radius will grow larger than $\lambda_T$. This situation still results in ignition, however, as the mass-energy $\sim 10$ GeV released per ion is much larger than the $\sim$ MeV needed per ion for fusion. Note finally that the Q-ball interaction described above results in minimal slowing for Q-balls this massive, so transits will easily penetrate the non-degenerate WD envelope (13).

The existing limits on Q-balls primarily come from Super-Kamiokande and air fluorescence detectors of cosmic rays (OA, TA) [34]. However, the constraints that come from considering the ignition of WDs are in a fundamentally new and complementary region of parameter space. These are plotted in Figure 12. We have also included the constraints that result from gravitational heating of a WD during a Q-ball transit, as in [1].

## VII. DISCUSSION

The detection of ultra-heavy DM is an open problem which will likely require a confluence of astrophysical probes. Here we present a guide to constraining these DM candidates through inelastic scatters, annihilations, and decays inside a WD that release sufficient SM energy to trigger runaway fusion. In particular, we calculate the energy loss of

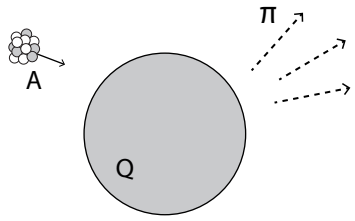


FIG. 11: Interaction of a baryonic Q-ball with a nucleus $A$. The Q-ball destroys the nucleus and absorbs its baryonic charge, while the excess energy is radiated into roughly $A$ outgoing pions of energy $\Lambda_{\rm QCD}$.

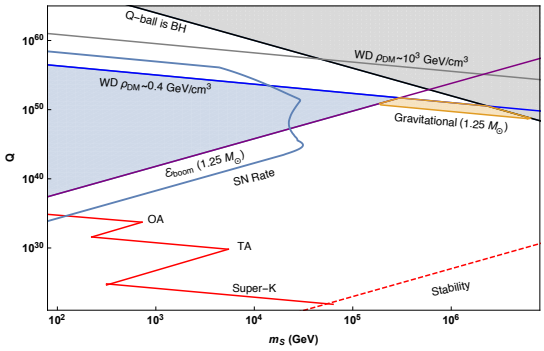


FIG. 12: Constraints on Q-ball DM. Bounds come from demanding that the Q-ball interaction during a DM transit is capable of igniting WDs, occurring at a rate large enough to either ignite a single observed 1.25 $M_\odot$ WD in its lifetime (WD in local DM density is blue shaded) or exceed the measured SN rate in our galaxy. Also shown is the corresponding constraint from gravitational heating of WDs (orange shaded), and existing limits from terrestrial detectors (red) [34].

high-energy particles due to SM interactions within the WD medium and determine the conditions for which a general energy deposition will heat a WD and ignite SN. Ultra-heavy DM that produces greater than $10^{15}$ GeV of SM particles in a WD is highly constrained by the existence of heavy WDs and the measured SN rate. The formalism provided will enable WDs to be applied as detectors for any DM model capable of heating the star through such interactions. We have done so for baryonic Q-balls, significantly constraining the allowed parameter space in a complementary way to terrestrial searches.

We have explored very briefly the application of this WD instability to self-gravitational collapse of DM cores, which has very interesting possibilities. Such collapsing cores can produce enough heating via multiple annihilations to ignite the star for much smaller DM masses than those considered here, e.g. $10^7$ GeV and can induce SN through other means such as the formation and evaporation of mini black holes. These will be addressed in future work [21].

Finally, in addition to the constraints mentioned above, the general phenomenology of these DM-induced runaways will be the ignition of sub-Chandrasekhar mass WDs. This raises the tantalizing possibility that DM encounters with WDs provide an alternative explosion mechanism for type 1a SN. For decades it had been widely regarded that type 1a SN are caused by accretion onto carbon-oxygen WDs in binary systems that reach the critical $\approx 1.4\ M_\odot$ Chandrasekhar mass limit, although it is now understood that such a process cannot account for all observed SN. Recent observations [5, 6] suggest that an $\mathcal{O}(1)$ fraction of the observed type 1a SN appear to have sub-Chandrasekhar progenitors. While other mechanisms exist to explain these SN [7, 8] [9], in light of the lack of understanding of DM and its interactions, it is worthwhile to consider whether DM encounters with WDs may also give rise to type 1a SN progenitor.

## A. PARTICLE STOPPING IN A WHITE DWARF

Here we provide a more detailed analysis of the stopping power (energy loss per distance traveled) of high-energy SM particles in a carbon-oxygen WD due to strong and electromagnetic interactions. We consider incident electrons, photons, pions, and nucleons with kinetic energy greater than an MeV.

### 1. WD Medium

For the WD masses that we consider, the stellar medium consists of electrons and fully-ionized carbon nuclei with central number densities in the range $n_e = Z n_{\rm ion} \sim 10^{31} - 10^{33}$ cm$^{-3}$ where $Z = 6$. The internal temperature is $T \sim$ keV [15]. The electrons are a degenerate and predominantly relativistic free gas, with Fermi energy

$$E_F = (3\pi^2 n_e)^{1/3} \sim 1 - 10 \text{ MeV}. \tag{37}$$

The carbon ions, however, are non-degenerate and do not form a free gas. The plasma frequency due to ion-ion Coulomb interactions is given by

$$\Omega_p = \left( \frac{4\pi n_{\rm ion} Z^2 \alpha}{m_{\rm ion}} \right)^{1/2} \sim 1 - 10 \text{ keV}, \tag{38}$$

where $m_{\rm ion}$ is the ion mass. Finally, the medium also contains thermal photons, though these are never significant for stopping particles as the photon number density $n_\gamma \sim T^3$ is much smaller than that of electrons or ions.

### 2. Nuclear Interactions

*a. Elastic Scattering of Hadrons.* Hadrons with energy less than the nuclear binding energy $E_{\rm nuc} \sim 10$ MeV will predominantly stop due to elastic nuclear scatters with ions. These are hard scatters, resulting in a stopping power

$$\frac{dE}{dx} \sim n_{\rm ion} \sigma_{\rm el} \left( \frac{m}{m_{\rm ion}} \right) E \tag{39}$$

for a hadron of mass $m \ll m_{\rm ion}$ and kinetic energy $E$. $\sigma_{\rm el}$ is the elastic nuclear scattering cross-section, which is of order $\sigma_{\rm el} \approx$ b at these energies and drops to $\sigma_{\rm el} \approx 0.1$ b above 10 MeV [35], ignoring the nontrivial effect of nuclear resonances in the intermediate regime $1 - 10$ MeV.

*b. Inelastic Scattering of Hadrons.* For energies above $E_{\rm nuc}$, the stopping of hadrons is dominated by inelastic nuclear scatters. In such a collision, an incoming hadron interacts with one or more nucleons to produce a $\mathcal{O}(1)$ number of additional hadrons which approximately split the initial energy. At incident energy greater than $\sim$ GeV, the majority of secondary hadrons are pions with transverse momenta $\sim 100$ MeV [35]. Below $\sim$ GeV, it is found that roughly equal fractions of protons, neutrons, and pions are produced in each collision [36]. We will thus have a roughly collinear shower terminating at an energy $\sim 10$ MeV which consists of pions for most of the shower's development and converts to an mix of pions and nucleons in the final decade of energy. This cascade is described by a radiative stopping power

$$\frac{dE}{dx} \sim n_{\rm ion} \sigma_{\rm inel} E, \tag{40}$$

where the inelastic nuclear cross-section is given by $\sigma_{\rm inel} \approx 100$ mb and roughly constant in energy [35]. The total length of the shower is only logarithmically dependent on the initial hadron energy $E$,

$$X_{\rm had} \sim \frac{1}{n_{\rm ion} \sigma_{\rm inel}} \log \left( \frac{E}{E_{\rm nuc}} \right). \tag{41}$$

(Note, in Figure 3, we have added 1 to the argument of the log to avoid divergence.)

*c. Photonuclear Interactions.* Photons of energy greater than 10 MeV can also strongly interact with nuclei through the production of virtual quark-antiquark pairs. This is the dominant mode of photon energy loss at high energy. The photonuclear scatter destroys the photon and fragments the nucleus, producing secondary hadrons in a shower analogous to that described above. The photonuclear cross-section $\sigma_{\gamma A}$ is roughly given by $\sigma_{\gamma A} \approx \alpha \sigma_{\rm inel}$, again ignoring the nuclear resonances that occur for $E \lesssim$ GeV. [35] For $E \gtrsim$ GeV, $\sigma_{\gamma A}$ is likely a slowly increasing function of energy due to the coherent interaction of the photon over multiple nucleons [37], however, instead of extrapolating this behavior we conservatively take a constant photonuclear cross-section $\sigma_{\gamma A} \approx 1$ mb.

*d. Electronucelar Interactions.* Electrons can similarly lose energy to nuclei by radiating a virtual photon that undergoes a photonuclear scatter, which indeed provides the dominant energy loss for high energy electrons. The cross-section for this process is roughly given by the photonuclear cross-section, scaled by a factor representing the probability to radiate such a photon. This can be estimated with the Weizsacker-Williams approximation, which gives

a stopping power that is suppressed from the photonuclear result by $\alpha$ but enhanced by an $\mathcal{O}(10)$ logarithmic phase space factor [37]:

$$\frac{dE}{dx} \sim \alpha\, n_{\rm ion}\sigma_{\gamma A} E \log\left(\frac{E}{m_e}\right). \tag{42}$$

Unlike the photonuclear interaction, the electronuclear event is a radiative process that preserves the original electron while leaving hadronic showers in its wake.

### 3. Radiative Processes

Electromagnetic showers due to successive bremsstrahlung and pair production events off carbon ions are the dominant stopping mechanisms for intermediate-energy electrons and photons. Both of these processes result in radiative stopping powers, derived semi-classically as [38]

$$\frac{dE}{dx} \sim \frac{E}{X_0}, \qquad X_0^{-1} = 4 n_{\rm ion} Z^2 \frac{\alpha^3}{m_e^2} \log\Lambda. \tag{43}$$

$X_0$ is the well-known radiation length, and $\log\Lambda$ is a Coulomb form factor given by the range of effective impact parameters $b$:

$$\Lambda = \frac{b_{\rm max}}{b_{\rm min}}. \tag{44}$$

The maximal impact parameter is set by the plasma screening length (see A 4 0 a) and the minimum by the electron mass, below which the semi-classical description breaks down. Note that for the highest WD densities $\Lambda \lesssim 1$, in which case (43) ought be replaced by a fully quantum mechanical result as in [39]. This still results in a radiative stopping power, and so for simplicity we employ (43) with $\log\Lambda \sim \mathcal{O}(1)$ for all WD densities.

*a. LPM Suppression* A radiative event involving momentum transfer $q$ to an ion must, quantum mechanically, occur over a length $\sim q^{-1}$. All ions within this region contribute to the scattering of the incident particle, and for sufficiently small $q$ this results in a decoherence that suppresses the formation of photons or electron-positron pairs. This is the "Landau-Pomeranchuk-Midgal" (LPM) effect. The momentum transfer $q$ in a given event decreases with increasing incident particle energy, and so the LPM effect will suppress radiative processes for energies greater than some scale $E_{\rm LPM}$. This can be calculated semi-classically [38],

$$E_{\rm LPM} = \frac{m_e^2 X_0 \alpha}{4\pi} \approx 1\ {\rm MeV}\left(\frac{10^{32}{\rm cm}^{-3}}{n_{\rm ion}}\right). \tag{45}$$

which is quite small due to the high ion density in the WD. The stopping power for bremsstrahlung and pair production in the regime of LPM suppression $E > E_{\rm LPM}$ is

$$\frac{dE}{dx} \sim \frac{E}{X_0}\left(\frac{E_{\rm LPM}}{E}\right)^{1/2} \qquad E > E_{\rm LPM}. \tag{46}$$

In addition to the LPM effect, soft bremsstrahlung may be suppressed in a medium as the emitted photon acquires an effective mass of order the plasma frequency $\Omega_p$. However, for high-energy electrons this dielectric suppression only introduces a minor correction to (46), in which soft radiation is already suppressed [38].

### 4. Elastic EM Scattering

*a. Electron Coulomb Scattering off Ions.* Coulomb collisions with ions are the mechanism by which electrons of energy $1 - 10$ MeV ultimately thermalize ions. In this scenario we may treat the ions as stationary and ignore their recoil during collisions. The nuclear charge will be screened by the mobile electrons of the medium, so incident particles scatter via a potential

$$V(\mathbf{r}) = \frac{Z\alpha}{r} e^{-\lambda_{\rm TF} r}. \tag{47}$$

The screening length $\lambda_{\rm TF}$ is given in the Thomas-Fermi approximation by [40]:

$$\lambda_{\rm TF}^2 = \frac{E_F}{6\pi\alpha n_e} \sim \frac{1}{\alpha E_F^2}. \tag{48}$$

This plasma screening suppresses scatters with momentum transfers below $\sim \lambda_{\rm TF}^{-1}$, corresponding to a minimal energy transfer of $\omega_{\rm min} = \lambda_{\rm TF}^{-2}/2m_{\rm ion}$. Ions may in principle also cause screening through lattice distortion, however this may be ignored as the sound speed of the lattice $c_s \sim 10^{-2}$ is much smaller than the speed of an incident relativistic electron. From the Born approximation, the cross-section for energy transfer $\omega$ is

$$\frac{d\sigma}{d\omega} = \frac{2\pi Z^2\alpha^2}{m_{\rm ion} v_{\rm in}^2} \frac{1}{(\omega+\omega_{\rm min})^2}, \tag{49}$$

where $v_{\rm in}$ is the incident velocity. Thus the stopping power is

$$\begin{aligned}\frac{dE}{dx} &= \int_0^{\omega_{\rm max}} d\omega\, n_{\rm ion} \frac{d\sigma}{d\omega}\omega \\ &\approx \frac{2\pi\, n_{\rm ion} Z^2\alpha^2}{m_{\rm ion} v_{\rm in}^2} \log\left(\frac{\omega_{\rm max}}{\omega_{\rm min}}\right),\end{aligned} \tag{50}$$

where the second line is valid if $\omega_{\rm max} \gg \omega_{\rm min}$. $\omega_{\rm max}$ is the maximum possible energy transfer. This may be due to 4-momentum conservation, or in the case of incident electrons, the impossibility of scattering to a final energy less than $E_F$. 4-momentum conservation sets an upper bound $\omega_{\rm kin}$, which for a stationary target is

$$\omega_{\rm kin} = \frac{2m_{\rm ion}p^2}{m_{\rm ion}^2 + m^2 + 2Em_{\rm ion}}, \tag{51}$$

with $p$, $E$ the incoming momentum and energy. The Fermi upper bound is $\omega_F = E - E_F$ so for incident electrons we take $\omega_{\rm max} = \min\{\omega_{\rm kin}, \omega_F\}$.

For scatters that transfer energy less than the plasma frequency $\Omega_p$, one may be concerned about phonon excitations. This occurs for incident electrons with energy below $\sim 10$ MeV. We estimate this stopping power treating each ion as an independent oscillator with frequency $\Omega_p$ (an Einstein solid approximation) and compute the stopping power due to scatters which excite a single oscillator quanta. There are two key differences between this and the free ion case: incident particles must transfer an energy $\Omega_p$, and the cross-section to transfer momentum $q$ is suppressed by a factor $q^2/2m_{\rm ion}\Omega_p = \omega_{\rm free}/\Omega_p$. $\omega_{\rm free}$ is the energy transfer that would accompany a free ion scatter with momentum transfer $q$. The resulting stopping power is unchanged from the free case (50), as the increased energy transfer compensates for the suppressed cross-section.

Finally, we note that for highly energetic incident particles the cross-section (49) should be modified to account for the recoil of the ion. However, at such energies the dominant stopping power will be from hadronic or electromagnetic showers anyway.

*b. Relativistic Coulomb Scattering off Electrons.* The scattering of incident electrons off degenerate electrons determines the termination energy of electromagnetic showers. This calculation demands two considerations not present when scattering off ions: the targets are not stationary and they require a threshold energy transfer in order to be scattered out of the Fermi sea. However for relativistic incident particle, with momentum $p \gg p_F$, the stopping power off electrons is ultimately of the same form as the stopping power off ions (50). In this limit, all particle velocities and the relative velocity is $\mathcal{O}(1)$, and the deflection of the incident particle will generally be small. It is reasonable then that scattering proceeds, up to $\mathcal{O}(1)$ factors, as though a heavy incident particle is striking a light, stationary target. The cross-section is given by the usual result,

$$\frac{d\sigma}{d\omega} \approx \frac{2\pi\alpha^2}{E_F}\frac{1}{\omega^2}, \tag{52}$$

where we have accounted for the target's motion by replacing its mass with its relativistic inertia $\approx E_F$. This is equivalent to a boost of the cross section from the rest frame of the target into the WD frame. Note that plasma screening can be ignored in this case, as Pauli-blocking will provide a more stringent cutoff on soft scatters. Scatters which transfer an energy $\omega \leq E_F$ will have a suppressed contribution to the stopping power as they can only access a fraction of the Fermi sea. In this limit it is sufficient to ignore these suppressed scatters:

$$\begin{aligned}\frac{dE}{dx} &= \int_{E_F}^{\omega_{\rm max}} d\omega\, n_e \frac{d\sigma}{d\omega}\omega \\ &\approx \frac{2\pi\, n_e\alpha^2}{E_F} \log\left(\frac{\omega_{\rm max}}{E_F}\right)\end{aligned} \tag{53}$$

where, as described above, $\omega_{\rm max} = \min\{\omega_{\rm kin}, \omega_F\}$. This derivation is admittedly quite heuristic, and so it has been checked with a detailed numerical calculation accounting fully for the target's motion and degeneracy. Equation (53) is indeed a good approximation to the stopping power for incident energies larger than the Fermi energy.

*c. Non-Relativistic Coulomb Scattering off Electrons* For non-relativistic incident particles, the Coulomb stopping off electrons becomes strongly suppressed due to degeneracy. Stopping in this limit appears qualitatively different than in the typical case—the slow incident particle is now bombarded by relativistic electrons from all directions. Note that only those scatters which slow the incident particle are allowed by Pauli-blocking.

As the electron speeds are much faster than the incident, a WD electron with momentum $p_F$ will scatter to leading order with only a change in direction, so the momentum transfer is $|\vec{q}| \sim p_F$. We again take the incident momentum $p \gtrsim p_F$, which is valid for all incident particles we consider. This results in an energy transfer

$$\omega = \left| \frac{p^2}{2m} - \frac{(\vec{p} - \vec{q})^2}{2m} \right| \sim v_{\rm in} E_F. \tag{54}$$

For $v_{\rm in} \ll 1$ the energy transfer is less than Fermi energy, so Pauli-blocking will be important. The incident particle is only be able to scatter from an effective electron number density

$$n_{\rm eff} = \int_{E_F - \omega}^{E_F} g(E)\, dE \approx 3 n_e \frac{\omega}{E_f}, \tag{55}$$

where $g(E)$ is the Fermi density of states. At leading order the electron is not aware of the small incident velocity, so the cross section is given by relativistic Coulomb scattering off a stationary target $\sigma \sim \alpha^2/q^2$ [41]. The incident particle thus loses energy to degenerate electrons at a rate:

$$\frac{dE}{dt} \sim n_{\rm eff}\, \sigma\, \omega \sim n_e \frac{\alpha^2}{E_F} v_{\rm in}^2. \tag{56}$$

Note that this includes a factor of the relative velocity which is $\mathcal{O}(1)$. As a result, the stopping power is parametrically

$$\frac{dE}{dx} = \frac{1}{v_{\rm in}} \frac{dE}{dt} \sim n_e \frac{\alpha^2}{E_F} v_{\rm in}. \tag{57}$$

As above, this heuristic result has been verified with a full integration of the relativistic cross section.

We can compare (57) to the stopping power of non-relativistic, heavy particles off roughly stationary, non-degenerate electrons $\frac{dE}{dx} \sim n_e \frac{\alpha^2}{m_e v_{\rm in}^2}$, which is the familiar setting of stopping charged particles in a solid due to ionization [42]. Evidently, the analogous stopping in a WD is parametrically suppressed by $v_{\rm in}^3 m_e/E_F$. One factor of $v_{\rm in}$ is due to Pauli blocking, while the other factors are kinematic, due to the relativistic motion of the targets.

*d. Compton Scattering* Compton scattering off degenerate electrons is the dominant interaction for photons of incident energy $k \leq E_F$. As we will show, this stopping power is parametrically different from that of high-energy photons due to Pauli-blocking and the motion of the electron. For $k > E_F$, the effect of Pauli-blocking is negligible and the stopping power is simply:

$$\frac{dk}{dx} \sim \frac{\pi \alpha^2 n_e}{E_F} \log\left(\frac{k}{m_e}\right), \tag{58}$$

where again we have (partially) applied the heuristic $m_e \to E_F$ replacement to boost the usual result for stationary electrons while avoiding divergence at the Fermi energy. This, along with the low-energy estimate below, matches a full integration of the relativistic cross section well.

We now turn to the regime of interest, $k < E_F$. Only those electrons near the top of the Fermi sea are available to scatter, so the photon interacts with only the effective electron density (55). In addition, Compton scatters will only occur off electrons moving roughly collinear with the photon momentum - a head-on collision would result in an energy loss for the electron, which is forbidden by Pauli exclusion. In the electron rest frame these collinear scatters are Thompson-like, and the photon energy loss is dominated by backward scatters. For relativistic electrons near the Fermi surface, these scatters transfer an energy

$$\omega \sim k \left(1 - \frac{m_e^2}{4E_F^2}\right) \approx k. \tag{59}$$

The cross section can be taken in the electron rest frame $\sigma \sim \alpha^2/m_e^2$, along with an 'aiming' factor $1/4\pi$ to account for the restriction to initially parallel trajectories. This gives a stopping power

$$\frac{dk}{dx} \approx \frac{\alpha^2 n_e k^2}{4\pi m_e^2 E_F}. \tag{60}$$

## B. DARK MATTER CAPTURE

Here we give a more detailed discussion of DM capture and its subsequent evolution in a WD.

### 1. Capture Rate

Consider a spin-independent, elastic scattering off ions with cross section $\sigma_{\chi A}$. For the DM to ultimately be captured, it must lose energy $\sim m_\chi v^2$, where $v$ is the DM velocity (in the rest frame of the WD) asymptotically far away. Since typically $v \ll v_{\rm esc}$, the DM has velocity $v_{\rm esc}$ while in the star and must lose a fraction $(v/v_{\rm esc})^2$ of its kinetic energy to become captured. Properly, the DM velocity is described by a boosted Maxwell distribution peaked at the galactic virial velocity $v_{\rm halo} \sim 10^{-3}$. However, this differs from the ordinary Maxwell distribution by only $\mathcal{O}(1)$ factors [19], and we can approximate it by (ignoring the exponential Boltzmann tail):

$$\frac{dn_\chi}{dv} \approx \begin{cases} \frac{\rho_\chi}{m_\chi}\left(\frac{v^2}{v_{\rm halo}^3}\right) & v \le v_{\rm halo} \\ 0 & v > v_{\rm halo} \end{cases}. \tag{61}$$

The DM capture rate is given by an integral of the DM transit rate weighted by a probability for capture $P_{\rm cap}$

$$\Gamma_{\rm cap} \sim \int dv \frac{d\Gamma_{\rm trans}}{dv} P_{\rm cap}(v), \tag{62}$$

where the (differential) transit rate is

$$\frac{d\Gamma_{\rm trans}}{dv} \sim \frac{dn_\chi}{dv} R_{\rm WD}^2 \left(\frac{v_{\rm esc}}{v}\right)^2 v. \tag{63}$$

$P_{\rm cap}$ depends on both the *average* number of scatters in a WD

$$\overline{N}_{\rm scat} \sim n_{\rm ion} \sigma_{\chi A} R_{\rm WD}, \tag{64}$$

and the number of scatters *needed* for capture

$$N_{\rm cap} \sim \max\left\{1, \frac{m_\chi v^2}{m_{\rm ion} v_{\rm esc}^2}\right\}, \tag{65}$$

and is most generally expressed as a Poisson sum

$$P_{\rm cap} = 1 - \sum_{n=0}^{N_{\rm cap}-1} \exp(-\overline{N}_{\rm scat}) \frac{(\overline{N}_{\rm scat})^n}{n!}. \tag{66}$$

For our purposes we will approximate the sum as follows:

$$P_{\rm cap} \approx \begin{cases} 1 & \overline{N}_{\rm scat} > N_{\rm cap} \\ \overline{N}_{\rm scat} & \overline{N}_{\rm scat} < N_{\rm cap} \text{ and } N_{\rm cap} = 1 \\ 0 & \text{else} \end{cases}. \tag{67}$$

Here we ignore the possibly of capture if $\overline{N}_{\rm scat} < N_{\rm cap}$ except in the special case that only one scatter is needed for capture. If $\overline{N}_{\rm scat} > N_{\rm cap}$, we assume all DM is captured. Most accurately, this capture rate should be computed numerically, e.g. see [43] for a detailed calculation. However with the above simplifications we find that the capture rate is of order

$$\Gamma_{\rm cap} \sim \Gamma_{\rm trans} \cdot \min\left\{1, \overline{N}_{\rm scat} \min\{B, 1\}\right\}, \tag{68}$$
$$B \equiv \frac{m_{\rm ion} v_{\rm esc}^2}{m_\chi v_{\rm halo}^2}.$$

$B$ here encodes the necessity of multiple scattering for capture. For ultra-heavy DM $m_\chi > 10^{15}$ GeV, $B \ll 1$ and essentially multiple scatters are always needed.

To compare with existing direct detection constraints, we relate $\sigma_{\chi A}$ to the per-nucleon cross section

$$\sigma_{\chi A} = A^2 \left(\frac{\mu_{\chi A}}{\mu_{\chi n}}\right)^2 F^2(q)\sigma_{\chi n} \sim A^4 F^2(q)\sigma_{\chi n}, \tag{69}$$

where $F^2(q)$ is the Helm form factor [16]. For DM at the WD escape velocity, the typical momentum transfer to ions is $q \sim \mu_{\chi A} v_{\rm esc} \sim 200$ MeV and the energy transfer is $q^2/m_{\rm ion} \sim$ MeV. As this $q$ is less than or of order the inverse nuclear size, DM scattering off nuclei will be coherently enhanced. We find $F^2(q) \approx 0.1$ for $q \sim 200$ MeV. Currently, the most stringent bound on DM spin-independent nuclear cross sections [17] is:

$$\sigma_{\chi n} < 5 \times 10^{-46}\ {\rm cm}^2 \left(\frac{m_\chi}{10^3\ {\rm GeV}}\right). \tag{70}$$

It follows that for any DM candidate satisfying (70), less than 1% of transiting DM is captured by the star. Therefore, in the regime of interest the capture rate scales as

$$\Gamma_{\rm cap} \propto \frac{\sigma_{\chi A}}{m_\chi^2}. \tag{71}$$

### 2. Thermalization and Collapse

For the remainder of this section all numerical quantities are evaluated at a central WD density $n_{\rm ion} \sim 10^{31}\ {\rm cm}^{-3}$, for which the relevant WD parameters are [12]:

$$\begin{aligned} M_{\rm WD} &\approx 1.25\ M_\odot \\ R_{\rm WD} &\approx 4000\ {\rm km} \\ v_{\rm esc} &\approx 2 \times 10^{-2}. \end{aligned} \tag{72}$$

Depending on the context, the relevant density may be the average value which is of order $n_{\rm ion} \approx 10^{30}\ {\rm cm}^{-3}$. We also assume a typical WD temperature $T \sim$ keV. In addition, for simplicity we take a fixed value of $\sigma_{\chi A}$ valid for the entire range of momentum transfers considered.

Once DM is captured, it thermalizes to an average velocity

$$v_{\rm th} \sim \sqrt{\frac{T}{m_\chi}} \approx 10^{-12} \left(\frac{m_\chi}{10^{16}\ {\rm GeV}}\right)^{-1/2}, \tag{73}$$

and settles to the thermal radius

$$\begin{aligned} R_{\rm th} &\sim \left(\frac{T}{G m_\chi \rho_{\rm WD}}\right)^{1/2} \\ &\approx 0.1\ {\rm cm} \left(\frac{m_\chi}{10^{16}\ {\rm GeV}}\right)^{-1/2}, \end{aligned} \tag{74}$$

where its kinetic energy balances against the gravitational potential energy of the (enclosed) WD mass. This thermalization time can be explicitly calculated for elastic nuclear scatters [20]. The stopping power due to such scatters is

$$\frac{dE}{dx} \sim \rho_{\rm WD} \sigma_{\chi A}\ v\ \max\{v, v_{\rm ion}\}, \tag{75}$$

where $v_{\rm ion} \sim \sqrt{\frac{T}{m_{\rm ion}}}$ is the thermal ion velocity. The max function indicates the transition between "viscous" and "inertial" drag. The DM first passes through the WD many times on a wide orbit until the size of its orbit decays to become contained in the star. This takes a time

$$\begin{aligned} t_1 &\sim \left(\frac{m_\chi}{m_{\rm ion}}\right)^{3/2} \frac{R_{\rm WD}}{v_{\rm esc}} \frac{1}{\overline{N}_{\rm scat}} \frac{1}{\max\{\overline{N}_{\rm scat}, 1\}^{1/2}} \\ &\approx 7 \times 10^{16}\ {\rm s} \left(\frac{m_\chi}{10^{16}\ {\rm GeV}}\right)^{3/2} \left(\frac{\sigma_{\chi A}}{10^{-35}\ {\rm cm}^2}\right)^{-3/2}. \end{aligned} \tag{76}$$

Subsequently, the DM completes many orbits within the star until dissipation further reduces the orbital size to the thermal radius. This occurs after a time

$$t_2 \sim \left(\frac{m_\chi}{m_{\rm ion}}\right)\frac{1}{n_{\rm ion}\sigma_{\chi A}}\frac{1}{v_{\rm ion}} \approx 10^{14}\ {\rm s}\left(\frac{m_\chi}{10^{16}\ {\rm GeV}}\right)\left(\frac{\sigma_{\chi A}}{10^{-35}\ {\rm cm}^2}\right)^{-1}. \tag{77}$$

There is an additional $\mathcal{O}(10)$ logarithmic enhancement of the timescale once the DM velocity has slowed below $v_{\rm ion}$. Note that $t_2$ is much larger than the time to complete a single orbit, which is simply the gravitational free-fall timescale:

$$t_{\rm ff} \sim \sqrt{\frac{1}{G\rho_{\rm WD}}} \approx 0.5\ {\rm s}. \tag{78}$$

The DM will begin steadily accumulating at $R_{\rm th}$ after a time $t_1 + t_2$. Once the collected mass of DM at the thermal radius exceeds the WD mass within this volume, there is the possibility of self-gravitational collapse. The time to collect a critical number of DM particles is

$$t_{\rm sg} \sim \frac{\rho_{\rm WD}R_{\rm th}^3}{m_\chi\Gamma_{\rm cap}} \approx 10^{10}\ {\rm s}\left(\frac{m_\chi}{10^{16}\ {\rm GeV}}\right)^{-1/2}\left(\frac{\sigma_{\chi A}}{10^{35}\ {\rm cm}^2}\right)^{-1}, \tag{79}$$

which in the regime of ultra-heavy DM is much smaller than the decay and thermalization scales $t_1$ and $t_2$. Typically, the timescale for collapse is set by the DM sphere's ability to cool and shed gravitational potential energy. This is initially just $t_2$, while the time to collapse at any given radius $r$ decreases once the DM velocity rises again above $v_{\rm ion}$

$$t_{\rm cool} \sim t_2 {\rm min}\{v_{\rm ion}/v_\chi, 1\} \qquad v_\chi \sim \sqrt{\frac{GNm_\chi}{r}}, \tag{80}$$

where $N$ is the number of collapsing DM particles. However, since the DM collection timescale is shorter than the cooling time $t_{\rm sg} < t_2$, the dynamics of the collapse is initially set by further collection and adiabatic shrinking of the DM sphere. This over-collection will necessarily increase the number of collapsing DM particles beyond $\Gamma_{\rm cap}t_{\rm sg}$ and hasten the collapse until the collection time matches the cooling time.

**Acknowledgements**

We would like to thank Keisuke Harigaya, Spencer Klein, Jacob Leedom, Junsong Lin and Lian-Tao Wang for stimulating discussions.

[1] P. W. Graham, S. Rajendran and J. Varela, Phys. Rev. D **92**, no. 6, 063007 (2015) [arXiv:1505.04444 [hep-ph]].
[2] D. S. Akerib *et al.* [LUX Collaboration], Phys. Rev. Lett. **118**, no. 2, 021303 (2017) [arXiv:1608.07648 [astro-ph.CO]].
[3] R. Agnese *et al.* [SuperCDMS Collaboration], Phys. Rev. Lett. **120**, no. 6, 061802 (2018) [arXiv:1708.08869 [hep-ex]].
[4] K. Griest, A. M. Cieplak and M. J. Lehner, Astrophys. J. **786**, no. 2, 158 (2014) [arXiv:1307.5798 [astro-ph.CO]].
[5] R. Scalzo *et al.* [Nearby Supernova Factory Collaboration], Mon. Not. Roy. Astron. Soc. **440**, no. 2, 1498 (2014) [arXiv:1402.6842 [astro-ph.CO]].
[6] R. A. Scalzo, A. J. Ruiter and S. A. Sim, Mon. Not. Roy. Astron. Soc. **445**, no. 3, 2535 (2014) [arXiv:1408.6601 [astro-ph.HE]].
[7] S. E. Woosley and T. A. Weaver, Astrophysical Journal **423**, pp.371-379 (1994).
[8] M. Fink, W. Hillebrandt and F. K. Roepke, Astron. Astrophys. [Astron. Astrophys. **476**, 1133 (2007)] [arXiv:0710.5486 [astro-ph]].
[9] R. Pakmor, M. Kromer and S. Taubenberger, Astrophys. J. **770**, L8 (2013) [arXiv:1302.2913 [astro-ph.HE]].
[10] F. X. Timmes and S. E. Woosley, Astro. Phys. Journal **396**, 649 (1992).
[11] L. R. Gasques, A. V. Afanasjev, E. F. Aguilera, M. Beard, L. C. Chamon, P. Ring, M. Wiescher and D. G. Yakovlev, Phys. Rev. C **72**, 025806 (2005) [astro-ph/0506386].

[12] F. X. Timmes, link
[13] R. Gandhi, C. Quigg, M. H. Reno and I. Sarcevic, Phys. Rev. D **58**, 093009 (1998) [hep-ph/9807264].
[14] J. A. Formaggio and G. P. Zeller, Rev. Mod. Phys. **84**, 1307 (2012) [arXiv:1305.7513 [hep-ex]].
[15] R. Kippenhahn and A. Weigert, "Stellar Structure and Evolution, Springer (1994).
[16] R. H. Helm, Phys. Rev. **104**, 1466 (1956).
[17] E. Aprile *et al.* [XENON Collaboration], Phys. Rev. Lett. **119**, no. 18, 181301 (2017) [arXiv:1705.06655 [astro-ph.CO]].
[18] W. H. Press and D. N. Spergel, Astrophys. J. **296**, 679 (1985).
[19] A. Gould, Astrophys. J. **321**, 571 (1987).
[20] C. Kouvaris and P. Tinyakov, Phys. Rev. D **83**, 083512 (2011) [arXiv:1012.2039 [astro-ph.HE]].
[21] R. Janish, V. Narayan, and P. Riggins, in preparation
[22] S. Mereghetti, arXiv:1302.4634 [astro-ph.HE].
[23] S. J. Kleinman, S. O. Kepler, D. Koester, I. Pelisoli *et al.*, Astrophys. J. Suppl. **204**, article id. 5, 14 pp. (2013)
[24] K. Perez, C. J. Hailey, F. E. Bauer, *et al.*, Nature **520**, 646 (2015)
[25] F. Nesti and P. Salucci, JCAP **1307**, 016 (2013) [arXiv:1304.5127 [astro-ph.GA]].
[26] S. Chandrasekhar, "An Introduction to the Study of Stellar Structure", University of Chicago press (1939).
[27] A. Aab *et al.* [Pierre Auger Collaboration], JCAP **1508**, 049 (2015) [arXiv:1503.07786 [astro-ph.HE]].
[28] T. Abu-Zayyad *et al.* [Telescope Array Collaboration], Astrophys. J. **768**, L1 (2013) [arXiv:1205.5067 [astro-ph.HE]].
[29] S. W. Randall, M. Markevitch, D. Clowe, A. H. Gonzalez and M. Bradac, Astrophys. J. **679**, 1173 (2008) [arXiv:0704.0261 [astro-ph]].
[30] V. Poulin, P. D. Serpico and J. Lesgourgues, JCAP **1608**, no. 08, 036 (2016) [arXiv:1606.02073 [astro-ph.CO]].
[31] S. R. Coleman, Nucl. Phys. B **262**, 263 (1985) Erratum: [Nucl. Phys. B **269**, 744 (1986)].
[32] A. Kusenko and M. E. Shaposhnikov, Phys. Lett. B **418**, 46 (1998) [hep-ph/9709492].
[33] A. Kusenko, V. Kuzmin, M. Shaposhnikov, P. G. Tinyakov, Phys. Rev. Lett. **80**, 15 (1998) [hep-ph//9712212].
[34] M. Dine and A. Kusenko, Rev. Mod. Phys. **76**, 1 (2003) [hep-ph/0303065].
[35] S. Tavernier, "Experimental Techniques in Nuclear and Particle Physics", Springer (2010).
[36] T. S. H. Lee and R. P. Redwine, Annu. Rev. Nucl. Part. Sci **52**, pp.23-63 (2002)
[37] L. Gerhardt and S. R. Klein, Phys. Rev. D **82**, 074017 (2010) [arXiv:1007.0039 [hep-ph]].
[38] S. Klein, Rev. Mod. Phys. **71**, 1501 (1999) [hep-ph/9802442].
[39] H. Bethe and W. Heitler Proc. R. Soc. Lond. A 1934 146 83-112
[40] S. L. Shapiro and S. A. Teukolsky, "Black Holes, White Dwarfs, and Neutron Stars", Wiley (1983).
[41] J. D. Jackson, "Classical Electrodynamics", 3rd edition, John Wiley and Sons, New York, (1998).
[42] B. Rossi, "High Energy Particles", Prentice-Hall, Inc., Englewood Cliffs, NJ (1952).
[43] J. Bramante, A. Delgado and A. Martin, Phys. Rev. D **96**, no. 6, 063002 (2017) [arXiv:1703.04043 [hep-ph]].